

Random copolymerization of polythiophene for simultaneous enhancement of in-plane and out-of-plane charge transport for organic transistors and perovskite solar cells

Seong Yeon Ko¹ | Benjamin Nketia-Yawson² | Hyungju Ahn³ |
Jea Woong Jo²  | Min Jae Ko¹

¹Department of Chemical Engineering,
Hanyang University, Seoul, South Korea

²Department of Energy and Materials
Engineering and Research Center for
Photoenergy Harvesting & Conversion
Technology (phct), Dongguk University,
Seoul, Republic of Korea

³Pohang Accelerator Laboratory, Pohang,
Republic of Korea

Correspondence

Jea Woong Jo, Department of Energy and
Materials Engineering and Research
Center for Photoenergy Harvesting &
Conversion Technology (phct), Dongguk
University, 30 Pildong-ro, 1-gil, Jung-gu,
Seoul 04620, Republic of Korea.
Email: whwp78@dongguk.edu

Min Jae Ko, Department of Chemical
Engineering, Hanyang University,
222 Wangsimni-ro, Seongdong-gu, Seoul
04763, South Korea.
Email: mjko@hanyang.ac.kr

Funding information

Industry and Energy of the Republic of
Korea, Grant/Award Number:
2018201010636A; National Research
Foundation of Korea, Grant/Award
Numbers: NFR-2020R1G1A1011577, NRF-
2019R1F1A1059791; National Research
Foundation under the Ministry of Science
and ICT, the Republic of Korea, Grant/
Award Numbers: 2017M1A2A2087353,
2018R1A2B2006708

Summary

High-performance conjugated polymers for electronic applications can be developed by modulating an appropriate chemical structure that optimizes their crystal characteristics and charge-transport behavior. Herein, we demonstrated the simultaneous enhancement of the in-plane and out-of-plane charge transport of polythiophenes by random polymerization. We synthesized a polythiophene polymer by varying the ratio of two different dialkyl-substituted bi-thiophene and triethylene glycol-substituted mono-thiophene units; this polymer exhibited weakened orientation preferences of polymer crystallite films, a denser packing, and a more homogeneous surface morphology in comparison with its homopolymer analogue. Furthermore, this optimized random polymer afforded an enhanced in-plane mobility of $7.72 \text{ cm}^2 \text{ V}^{-1} \text{ second}^{-1}$, measured by field-effect transistor, and out-of-plane mobility of $8.86 \times 10^{-4} \text{ cm}^2 \text{ V}^{-1} \text{ second}^{-1}$, measured by space-charge-limited-current device. These are respectively 2.4 times and 10 times higher than the mobilities of the homopolymer (field-effect mobility = $3.25 \text{ cm}^2 \text{ V}^{-1} \text{ second}^{-1}$ and space-charge-limited-current mobility = $8.73 \times 10^{-5} \text{ cm}^2 \text{ V}^{-1} \text{ second}^{-1}$). The enhanced charge transport in out-of-plane direction was also confirmed by fabricating perovskite solar cells using optimized polythiophene as a hole-transporting material, which exhibited a higher efficiency of nearly 16.2% than the device with homopolymer analogue (12.0%).

KEYWORDS

charge-transport anisotropy, conjugated polymer, organic field-effect transistors, perovskite photovoltaics, polythiophene, random polymerization

Seong Yeon Ko and Benjamin Nketia-Yawson contributed equally to this work.

1 | INTRODUCTION

Semiconducting conjugated polymers (SCPs) have been extensively explored in electronics, owing to their unique properties including cost-effective manufacturing based on low-temperature solution processability, light weight, and mechanical deformability. Numerous studies on the electronic applications of SCPs, such as light-emitting diodes, photovoltaics, field-effect transistors, and chemical sensors, have reported that the chemical structures of the conjugated backbones and the attached side chains of SCPs meaningfully affect their optoelectrical properties. Hence, the SCPs should be specifically designed to realize high-performance operations in electronic devices.^{1–8} Particularly, the crystal characteristic requirements, including crystal structure, intermolecular distance, and orientation, vary according to the required charge-transporting ability of SCPs in electronic applications. For example, organic solar cells are fabricated based on the perpendicularly stacked device architecture, and therefore the face-on orientation of the SCP in the photoactive layer has been intensively studied to enhance the out-of-plane (OOP) charge transport, which facilitates the collection of charge carriers at the electrodes. Contrastingly, in organic field-effect transistors (OFETs), the edge-on crystal orientation of the SCP is preferred in the channels for efficient in-plane (IP) transport of charge carriers between source/drain electrodes. Hence, an SCP that has been designed to satisfy a specific application may not be able to typically achieve high performance in other types of electronic devices, because of the mismatch of the crystal property.

Thus far, several strategies for structural design, such as an alternating electron donor-acceptor conjugated structure, optimization of side-chain, non-covalently conformational locking, and halogenations, have emerged for modulating the crystal and charge-transport properties of SCPs.^{9–21} Another attractive approach toward developing high-performance SCPs for electronic devices is that of random copolymerization, which refers to the grouping of multiple different conjugated moieties into a single polymer backbone by varying the composition ratios. Random copolymerization has been demonstrated to tune the light absorption/emission ability, solubility, molecular ordering, frontier energy levels, and charge-carrier transport in SCPs by selecting appropriate combinations of different monomers. Moreover, recent studies have reported that random copolymerization could induce unexpected changes in the aggregation behavior and interchain alignment of the SCP backbones, which could be attributed to the random configuration of the diverse monomers. This randomness in polymer packing would provide different crystal characteristics and

charge-transport behaviors in the polymer films, which are not observed in the homopolymers synthesized using repeated structural units.^{22–27} Therefore, random copolymerization is deemed a possible approach to develop a highly charge transportable SCPs in various directions, which is a required factor for multiple electronic applications.

Herein, we demonstrate that the IP and OOP charge-transporting abilities of polythiophene SCPs are simultaneously enhanced by random polymerization. We synthesize polythiophenes by changing the ratio of two different dialkyl-substituted bi-thiophene (2R-BT) and triethylene glycol-substituted monothiophene (TEG-T) units in order to identify the influences of random polymerization with different thiophene units on the molecular ordering and charge-transport behavior of SCPs. Random polymers exhibit weakened orientational preferences of polymer crystallites in the film state, while the homopolymer synthesized using only the 2R-BT unit exhibits a more intensive tendency toward edge-on orientation. However, the optimized random polymer is observed to provide a denser packing and a more homogeneous morphology, and therefore afford improved charge-transporting abilities in both the IP and OOP directions, as evidenced by the systematic studies using OFETs, hole-only space-charge-limited-current (SCLC) devices, and perovskite solar cells (PSCs). As a result, it was verified that random polymerization is able to finely tune the charge transports of SCPs in diverse directions and is an attractive method to develop SCPs for multiple electronic applications.

2 | RESULTS AND DISCUSSION

As shown in Figure 1, one homopolymer (P0) and three random copolymers (2R-BT:TEG-T = 9:1, 8:2, and 7:3 for P10, P20, and P30, respectively) were prepared using Stille polymerization with Pd(PPh₃)₄ catalyst. 2-Octyldodecyl side groups were attached to 2R-BT monomer for improving the solubility of SCPs in organic solvents, while a polar and hydrophilic triethylene glycol (TEG) side group was chosen for the TEG-T monomer to obtain random copolymers with improved molecular ordering and interaction with the ionic compounds.^{28,29} Furthermore, difluorinated-bithiophene (2F-BT) monomer was introduced as a counterpart of the SCPs to obtain deeper energy levels of highest occupied molecular orbital (HOMO), improved planarity of conjugated backbones, and enhanced intermolecular interactions of polymer chains.^{30–33} We also attempted to synthesize the SCPs with higher TEG-T monomer content (2R-BT:TEG-T = 6:4 and 5:5), however, those SCPs showed limited

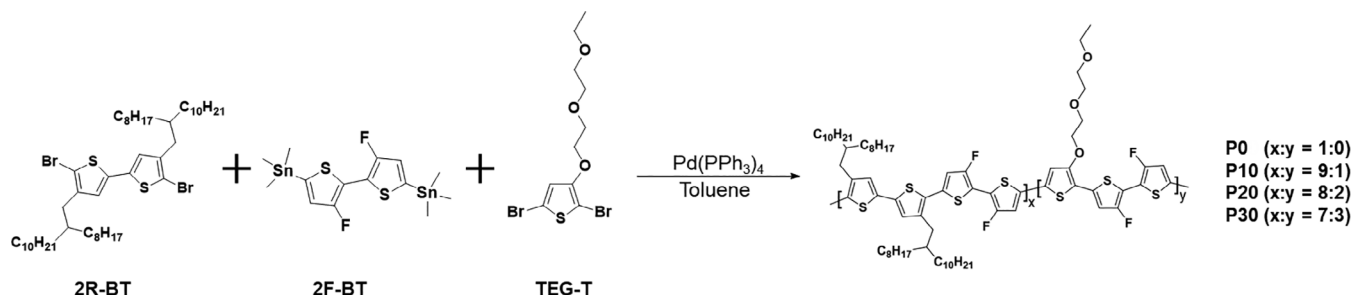


FIGURE 1 Synthesis of P0, P10, P20, and P30 polymers

SCP	M_n (kDa)	PDI	HOMO ^a (eV)	LUMO ^b (eV)	$E_{g,opt}$ ^c (eV)
P0	17.8	2.58	-5.32	-3.36	1.96
P10	16.5	2.87	-5.32	-3.37	1.95
P20	12.7	2.76	-5.29	-3.37	1.92
P30	15.6	2.59	-5.26	-3.39	1.87

TABLE 1 Molecular weights and energy levels of synthesized polythiophenes

Abbreviations: HOMO, highest occupied molecular orbital; LUMO, lowest unoccupied molecular orbital; PDI, polydispersity index; SCP, semiconducting conjugated polymers.

^aObtained from Figure S1A.

^bCalculated by $HOMO - E_{g,opt}$.

^cCalculated from Figure 2A.

solubility and processability. Thus, we studied the effects of random polymerization on the charge transport of SCPs by focusing on the comparison of P0, P10, P20, and P30 polymers. The number of average molecular weights (M_n) of SCPs, estimated by gel permeation chromatography (GPC), is in the range of 12.7 to 17.8 kDa with polydispersity index (PDI) in the range of 2.58 to 2.87, as listed in Table 1. Furthermore, the HOMO energy levels of P0, P10, P20, and P30 SCPs are -5.32, -5.32, -5.29, and -5.26 eV, respectively, indicating that all SCPs have appropriate HOMO energy levels for effective hole extraction at the hole-transporting material (HTM)/perovskite interface in perovskite solar cells (valence band maximum of perovskite = -5.4 eV).³⁴ The slightly increased HOMO energy levels in the polymers with higher TEG-T monomer content are possibly because of the electron-donating nature of the TEG side group. Moreover, the energy levels of the lowest unoccupied molecular orbital (LUMO) were extracted from the optical bandgaps and HOMO energy levels: all polymers are observed to have similar values of approximately -3.37 eV, resulting in a sufficient electron-blocking ability to prevent the undesirable transfer of electrons at the HTM/perovskite interface.³⁵ In addition, high thermal stabilities of synthesized polymers were revealed in thermogravimetric analysis (TGA) (Figure S1B): The weight of all polymers was well-conserved without thermal degradation under 350°C.

The influences of random polymerization on the polymer ordering of synthesized SCPs were explored by UV-Vis spectroscopy (Figure 2A). All synthesized polymers exhibited vibronic shoulders at around 600 nm, representing the existence of molecular ordering and aggregation of the SCPs in the film state.³⁶ Furthermore, P20 and P30, the random copolymers, exhibited distinct vibronic shoulders of similar intensity in comparison with the homopolymer P0, indicating that the former can form a highly ordered structure despite random copolymerization. However, the intensity of the vibronic shoulder of P10 was lower than that of the other polymers, suggesting not only that the interchain interaction between the polymers of P10 is weaker than in the others, but also that adding a small quantity of different monomer would disrupt the ordering of the polymer chains.³⁷ Furthermore, the optical bandgaps of P0, P10, P20, and P30 polymers were observed to be 1.96, 1.95, 1.92, and 1.87 eV, respectively; the narrower bandgap observed for P30 is possibly due to the shallower energy levels of HOMO by the introduced electron-donating TEG side groups.

The crystal characteristics of the synthesized polymers were studied by GIXRD analysis (Figure S3). Figure 2B,C, respectively, show the OOP scan (q_z) and IP scan (q_{xy}) obtained from GIXRD data of SCP films. When estimated from the peaks of (100) diffraction in the q_z direction, the interchain distances of 21.2, 21.1, and

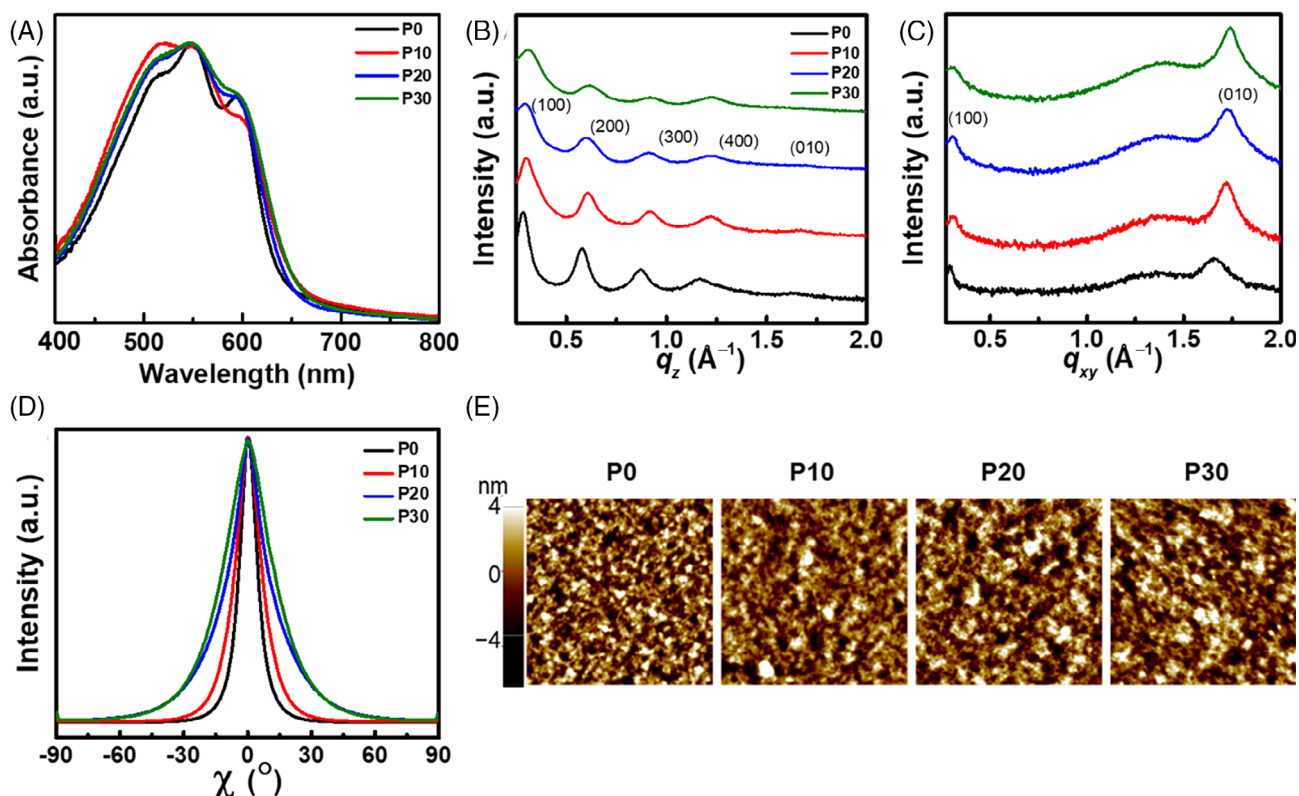


FIGURE 2 (A) UV-Vis absorption spectra of the SCP films. (B) q_z and (C) q_{xy} from GIXRD scans. (D) Azimuthal angle scans for the (100) diffraction peaks of P0, P10, P20, and P30 polymer film. (E) AFM topographic images of P0, P10, P20, and P30 polymer films ($2 \mu\text{m} \times 2 \mu\text{m}$) [Colour figure can be viewed at wileyonlinelibrary.com]

TABLE 2 Crystallographic parameters for SCP polymers

SCP	(100) Peak ^a (\AA^{-1})	$d_{(100)}$ ^a (\AA)	(010) Peak ^b (\AA^{-1})	$d_{(010)}$ ^b (\AA)	FWHM of (100) diffraction peak ^c ($^\circ$)
P0	0.28	22.2	1.66	3.78	9.1
P10	0.30	21.2	1.72	3.65	13.7
P20	0.30	21.1	1.73	3.64	23.9
P30	0.31	20.3	1.74	3.62	27.3

Abbreviations: FWHM, full-width-at-half-maximum; SCP, semiconducting conjugated polymers.

^aExtracted from Figure 2B.

^bExtracted from Figure 2C.

^cCalculated from Figure 2D.

20.3 \AA for P10, P20, and P30 polymers, respectively, were observed to be smaller than that of the homopolymer P0 (22.2 \AA) (Table 2). This may be because two long alkyl side chains of the random polymers are partially replaced with one short TEG group. The denser packing of the crystallites observed in the random polymers was further supported by the (010) diffractions in the q_{xy} profiles. The distances of π - π stacking calculated from the (010) diffraction peaks of the polymers were observed to be reduced from 3.78 \AA for P0 to 3.65, 3.64, and 3.62 \AA , respectively, for P10, P20, and P30 (Table 2). On the other hand, strong ($h00$) diffractions were observed in the q_z scans of

all polymer films, suggesting that the crystallites in all polymer films prefer an edge-on orientation. However, slightly different orientational orderings of polymer crystallites were observed in the azimuthal angle scans of the (100) reflection.^{38,39} As shown in Figure 2D, the full-width-at-half-maximum (FWHM) of the peaks at the azimuthal angle of 0° for P0, P10, P20, and P30 were 9.1, 13.7, 23.9, and 27.3 $^\circ$, respectively (Table 2). This would indicate that the orientation preferences of our SCPs are weakened and the random copolymerization of our polymers generates crystallites with mixed orientations.⁴⁰ Weakened orientation preferences after random copolymerization might

be related to the reduced regularity in conjugated backbone with two different monomeric units.⁴¹

Furthermore, the morphologies of the SCP films were explored by AFM. Figure 2E shows well-developed interconnected networks of nanoscale fibrils in all SCP films, although P20 exhibits a smoother, a more homogeneous morphology, and a slightly lower root-mean-square (RMS) surface roughness (RMS = 1.22, 1.64, 1.00, and 1.74 nm, respectively, for P0, P10, P20, and P30). This morphology of P20 is favorable for forming a better contact at the SCP/perovskite or SCP/metal electrode interfaces.³⁸ The increased RMS values in the P10 and P30 films could be due to the disruption of ordering (Figure 2A) and strong aggregation behavior (Figure 2B,C), respectively, causing the formation of inhomogeneous polymer films with unfavorable nucleation and crystallite growth.

The charge-transport behavior of the SCPs was identified by fabricating OFETs and hole-only SCLC devices. Figure 3A shows OFET with top-gate/bottom-contact (TGBC) configuration (channel length/width = 50 μm /1 mm) used for investigating the IP electrical properties of the synthesized SCPs, where a high-capacitance solid-state electrolyte gate insulator (SEGI) composed of P(VDF-HFP) (poly[vinylidene fluoride-co-hexafluoropropylene]) and [EMIM][TFSI] ionic liquid (1-ethyl-3-methylimidazolium bis[trifluoromethylsulfonyl]imide) was employed as a gate dielectric layer (Figure 3B). The SEGI layer was formed from the mixture of the P(VDF-HFP) solution and the P(VDF-HFP)/[EMIM][TFSI] gel solution (98:2 v/v ratio), which yielded a high capacitance of 21.86 $\mu\text{F cm}^{-2}$ (measured at 1 Hz using the metal/insulator/metal geometry), resulting from the combined formation of -C-F- dipole and electric double-layer through the polarization of SEGI.²⁸ Thus, not only a high charge-carrier density is induced at the semiconductor/gate dielectric interface, but also a low operating voltage is enabled in the OFETs.^{28,42} Figure 3C,D shows the OFET transfer and output curves of SCPs, and Table 3

summarizes their relevant device parameters. We attributed the low saturation behavior of the output characteristics to the short channel effect with the high channel width/length ratio, which is 20 (typically 10 in electrolyte-gated transistors).⁴³⁻⁴⁵ Hysteresis behavior was observed in the forward and reverse scan of the transfer characteristics of the SEGI-gated OFETs due to the ferroelectric nature, typical to those of conventional ion-gel transistors (Figure S4).⁴³ We measured relatively high gate leakage current (I_G) in the SEGI devices due to parasitic leakage pathways through the spin-coated SCPs layer around the contact electrodes (Figure S4). Patterning the active channel using strategic approaches such as photolithography or direct (inkjet) printing would decrease the I_G substantially. The random polymer P20 exhibited a higher average field-effect mobility ($\mu_{h,\text{FET}}$) of $4.57 \pm 1.34 \text{ cm}^2 \text{ V}^{-1} \text{ second}^{-1}$ than homopolymer P0 (average $\mu_{h,\text{FET}} = 2.49 \pm 0.59 \text{ cm}^2 \text{ V}^{-1} \text{ second}^{-1}$), with a maximum value of up to $7.72 \text{ cm}^2 \text{ V}^{-1} \text{ second}^{-1}$, which is ~ 2.4 times improved than that of P0 ($3.25 \text{ cm}^2 \text{ V}^{-1} \text{ second}^{-1}$). This enhancement in the $\mu_{h,\text{FET}}$ value is considered to be a consequence of the dense packing and smooth morphology of the P20 film (Figure 2B, C and E). However, P10 and P30 exhibited lower $\mu_{h,\text{FET}}$ values than P0, attributed to their high surface roughness. On the other hand, the SEGI-gated SCPs devices showed high charge mobilities compared to conventional OFETs with low-k poly(methyl methacrylate) (PMMA) dielectric. Fabricated homopolymer P0 and optimized P20 random copolymer SCPs PMMA-gated OFETs measured average hole mobility of 0.049 ± 0.003 and $0.065 \pm 0.099 \text{ cm}^2 \text{ V}^{-1} \text{ second}^{-1}$, respectively, attributing to lower charge-carrier density despite the high driving voltage of -80 V .⁴⁶

Figure 4A shows the hole-only SCLC device architecture used for measuring the OOP charge-transporting abilities of the SCPs.^{41,47} Furthermore, as shown in Figure 4B and Table 3, the random copolymers provided higher SCLC mobilities ($\mu_{h,\text{SCLC}}$) than the homopolymer P0, which

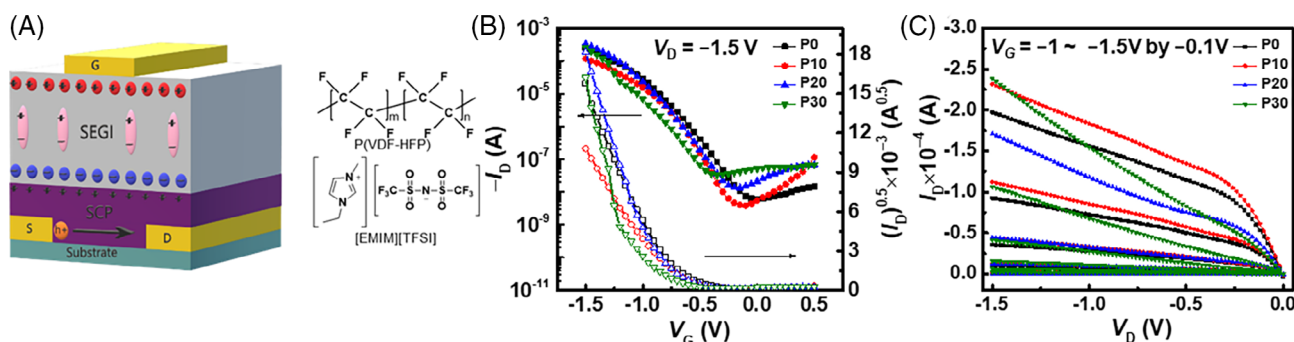


FIGURE 3 (A) Top-gate/bottom-contact OFET geometry for measuring the IP mobility of SCPs. (B) Chemical structures of P(VDF-HFP) and [EMIM][TFSI] used for preparing solid-state electrolyte gate insulator (SEGI) layer. (C) Transfer and (D) output curves of OFETs for P0, P10, P20, and P30 polymers [Colour figure can be viewed at wileyonlinelibrary.com]

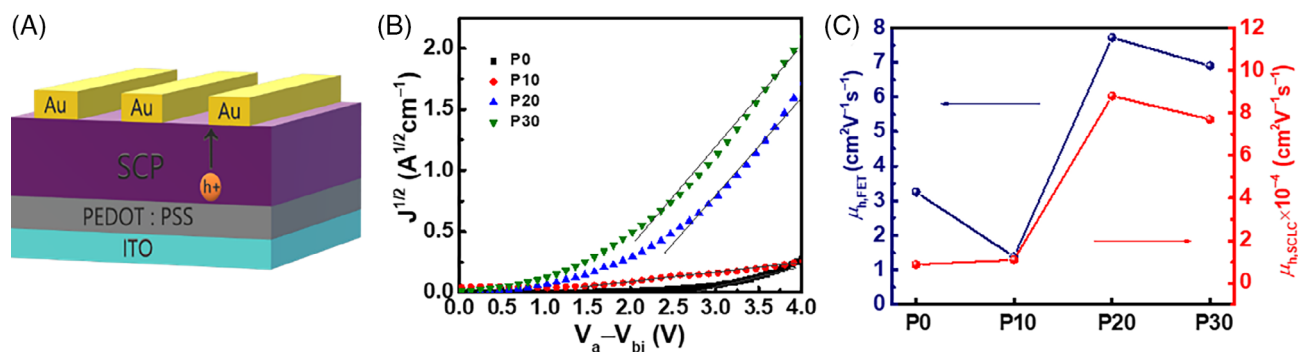


FIGURE 4 (A) Hole-only space-charge-limited-current (SCLC) device geometry for measuring the OOP mobility of SCPs. (B) Dark J - V curves of SCLC devices for P0, P10, P20, and P30; the linear fit of the data points are represented by the solid lines. (C) Comparison of IP and OOP mobilities of the SCPs obtained from the OFET and SCLC devices [Colour figure can be viewed at [wileyonlinelibrary.com](https://onlinelibrary.wiley.com/doi/10.1002/er.6293)]

TABLE 3 Electrical characteristics of P0, P10, P20, and P30 semiconducting conjugated polymer (SCPs)

SCP	$\mu_{h,FET}$ (Best) ($\text{cm}^2 \text{V}^{-1} \text{second}^{-1}$)	$\mu_{h,FET}$ (Ave.) ($\text{cm}^2 \text{V}^{-1} \text{second}^{-1}$) ^a	V_T (V)	$I_{on/off}$	$\mu_{h,SCLC}$ (Best) ($\times 10^{-4} \text{cm}^2 \text{V}^{-1} \text{second}^{-1}$)	$\mu_{h,SCLC}$ (Ave.) ($\times 10^{-4} \text{cm}^2 \text{V}^{-1} \text{second}^{-1}$) ^a
P0	3.25	2.49 ± 0.59	-0.97 ± 0.07	$>10^4$	0.87	0.77 ± 0.09
P10	1.38	0.95 ± 0.23	-0.94 ± 0.20	$>10^4$	1.15	1.03 ± 0.02
P20	7.72	4.57 ± 1.34	-1.08 ± 0.16	$>10^4$	8.86	6.91 ± 0.44
P30	6.90	3.72 ± 1.70	-0.99 ± 0.11	$>10^4$	7.78	6.34 ± 0.66

^aCalculated from at least eight devices.

indicates that the random polymers provide an improved charge transport in the direction of OOP, owing to the increased randomness in the crystal orientations of their films (Figure 2D). Moreover, P20 exhibited the highest $\mu_{h,SCLC}$ value of $8.86 \times 10^{-4} \text{cm}^2 \text{V}^{-1} \text{second}^{-1}$ and it has an order of magnitude higher than that of P0 ($0.87 \times 10^{-4} \text{cm}^2 \text{V}^{-1} \text{second}^{-1}$) (Figure 4C). The results of the above studies on the OFET and SCLC mobilities suggest that the introduction of random polymerization could simultaneously improve the IP as well as OOP charge-transporting abilities of the SCPs. We attribute the origin of simultaneous enhancement in both IP and OOP charge transport of P20 to closer distances of π - π and interchain stackings. (Table 2).

To ensure improvement in the charge transport of polythiophenes, the PSCs (ITO/SnO₂/(CS_{0.05}FA_{0.14}MA_{0.81})Pb(I_{0.86}Br_{0.14})₃/SCP(HTM)/Au) were also fabricated by employing the SCPs as HTMs, as shown in Figure 5A.^{48,49} The J - V curves of PSCs are displayed in Figure 5B and their solar cell properties are listed in Table 4. The PSCs using P20 and P30 HTMs exhibited similar and high average power conversion efficiencies (PCEs) of approximately 14.2%. This supports the observed higher hole mobilities of P20 and P30 polymers in the OOP direction (Figure 3F), which would provide the facilitated hole extraction from the perovskites and enhance hole-transport to the metal

electrode. Specifically, P20 exhibited the highest efficiency, with a PCE of 16.2% ($V_{OC} = 1.05 \text{V}$, $J_{SC} = 21.2 \text{mA cm}^{-2}$, $FF = 72.6\%$) while the PSCs using P0 and P10 exhibited device efficiencies of around 11.4%. This is due to the insufficient charge-transporting abilities of P0 and P10 causing an increase in the interface recombination and ineffective hole extraction at the HTM/perovskite interface, which reduces the J_{SC} and FF in PSCs. Furthermore, the reliability of the PSCs was verified by analyzing incidental photon-to-electron conversion efficiency (IPCE) spectra (Figure 5C). The J_{SC} determined by the integration of IPCE spectra were 18.6, 18.8, 21.0, and 19.5 mA cm^{-2} for P0, P10, P20, and P30, respectively, and these were consistent with the J_{SC} values measured in J - V curves. In addition, as shown in Figure 5D, the charge extraction/transport of SCPs was investigated by steady-state photoluminescence (PL). The perovskite films on P20 and P30 exhibited more efficient quenching of PL compared with those on P0 and P10, indicating the better hole-extraction abilities of P20 and P30 at the HTM/perovskite interface. Moreover, the perovskite films with P10, P20, and P30 random copolymers exhibited more blue-shifted PL emission peaks at 801 nm in comparison with the homopolymer P0 (803 nm). This shift could be a result of the reduced trap

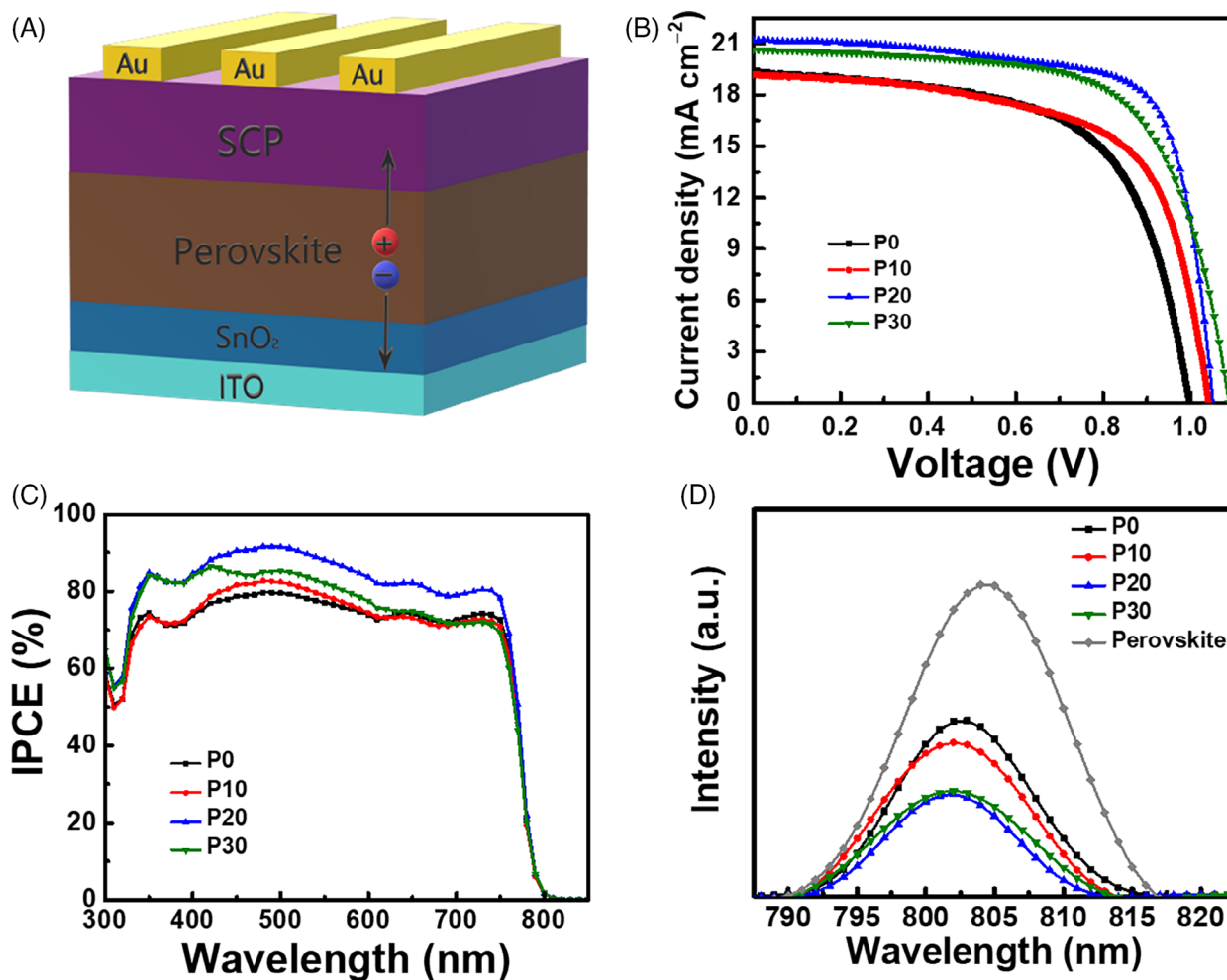


FIGURE 5 Comparison of hole extraction/transport abilities of semiconducting conjugated polymers (SCP) HTMs in PSCs. (A) Device architecture of the PSCs used in this study. (B) J - V curves and (C) IPCE spectra of PSCs using P0, P10, P20, and P30 SCPs as HTMs. (D) Steady-state PL spectra of the perovskite films deposited on bare glass and SCP films [Colour figure can be viewed at [wileyonlinelibrary.com](https://onlinelibrary.wiley.com/doi/10.1002/er.6293)]

TABLE 4 Device performances of perovskite solar cells prepared by employing semiconducting conjugated polymers (SCPs) as hole-transporting materials (150 nm)

SCP	PCE Best (Ave.) ^a (%)	V_{OC} Best (Ave.) ^a (V)	J_{SC} Best (Ave.) ^a (mA cm ⁻²)	FF Best (Ave.) ^a (%)
P0	12.0 (11.4 ± 0.4)	1.00 (0.97 ± 0.03)	19.2 (19.0 ± 0.5)	62.3 (60.3 ± 2.0)
P10	12.7 (11.4 ± 0.6)	1.04 (0.98 ± 0.03)	19.2 (19.1 ± 0.3)	64.1 (60.2 ± 2.1)
P20	16.2 (14.3 ± 0.5)	1.05 (0.99 ± 0.02)	21.2 (20.3 ± 0.2)	72.6 (69.3 ± 0.9)
P30	14.4 (14.0 ± 0.2)	1.00 (0.99 ± 0.02)	20.8 (20.1 ± 0.7)	69.2 (65.6 ± 1.8)

^aCalculated from at least 10 devices.

density due to the passivation effect of the triethylene glycol side chains attached to the polymers.⁵⁰⁻⁵³

3 | CONCLUSION

In summary, we synthesized polythiophene SCPs by the random copolymerization of two units, namely 2R-BT

and TEG-T, in different ratios. In comparison with the homopolymer synthesized 2R-BT (P0), the optimized random polymer P20 was observed to exhibit increased crystal orientation randomness, denser packing, and more homogeneous surface morphology. This improved its charge-transport abilities in both directions of IP and OOP, as verified by the OFETs and hole-only SCLC measurements. P20 exhibited an enhanced IP $\mu_{h,FET}$ of

7.72 cm² V⁻¹ second⁻¹ and OOP $\mu_{h,SCLC}$ of 8.86×10^{-4} cm² V⁻¹ second⁻¹, and these are respectively 2.4 times and 10 times improved values than those of the homopolymer P0 ($\mu_{h,FET} = 3.25$ cm² V⁻¹ second⁻¹ and $\mu_{h,SCLC} = 8.73 \times 10^{-5}$ cm² V⁻¹ second⁻¹). Furthermore, among the PSCs fabricated using the SCPs as the HTMs, P20 exhibited not only improved hole extraction/transport but also a higher PCE of up to 16.2% when compared to P0 (PCE = 12.0%). Moreover, the distinct change in the mobility in the direction of OOP in comparison with the direction of IP indicates a weakened orientation preference induced by the random copolymerization, which contributes to the development of a more efficient charge pathway in the former direction. Thus, our study demonstrates that the crystal properties can be tuned by utilizing a random polymerization, which paves a way for developing efficient charge-transporting SCPs in all directions, as required for the multiple electronic applications of the SCPs. This study provides insightful prospects for structural modification by random copolymerization strategy toward the development of versatile and high-performance SCPs, which are of primary importance for the fabrication of organic electronic devices—such as OFETs, organic photovoltaics, organic memories, and chemical sensors.

ACKNOWLEDGEMENTS

The authors thank the Ministry of Science and ICT (MSIT), Korea, for financial support by the National Research Foundation of Korea (NRF) grant (NRF-2019R1F1A1059791 and NRF-2020R1G1A1011577). This work is also supported by the Research Program (2018R1A2B2006708) and the Technology Development Program to Solve Climate Changes (2017M1A2A2087353) funded by the National Research Foundation under the Ministry of Science and ICT, the Republic of Korea. This work was also supported by the Korea Institute of Energy Technology Evaluation and Planning and the Ministry of Trade, Industry and Energy of the Republic of Korea (2018201010636A).

DATA ACCESSIBILITY

The data that support the findings of this study are available from the corresponding author upon reasonable request.

ORCID

Jea Woong Jo  <https://orcid.org/0000-0001-8086-2644>

REFERENCES

- Yamashita Y, Tsurumi J, Ohno M, et al. Efficient molecular doping of polymeric semiconductors driven by anion exchange. *Nature*. 2019;572:634-638.
- Berggren M, Malliaras GG. How conducting polymer electrodes operate. *Science*. 2019;364:233-234.
- Jiang C, Choi HW, Cheng X, Ma H, Hasko D, Nathan A. Printed subthreshold organic transistors operating at high gain and ultralow power. *Science*. 2019;363:719-723.
- Chen H, Hu Z, Wang H, et al. A chlorinated π -conjugated polymer donor for efficient organic solar cells. *Joule*. 2018;2:1623-1634.
- Chen CA, Yang PC, Wang SC, Tung SH, Su WF. Side chain effects on the optoelectronic properties and self-assembly behaviors of Terthiophene-Thieno[3,4-c]pyrrole-4,6-dione based conjugated polymers. *Macromolecules*. 2018;51:7828-7835.
- Nikolka M, Schweicher G, Armitage J, et al. Performance improvements in conjugated polymer devices by removal of water-induced traps. *Adv Mater*. 2018;30:1-8.
- Li M, Balawi AH, Leenaers PJ, et al. Impact of polymorphism on the optoelectronic properties of a low-bandgap semiconducting polymer. *Nat Commun*. 2019;10:1-11.
- Tenopala-Carmona F, Fronk S, Bazan GC, Samuel IDW, Carlos PJ. Real-time observation of conformational switching in single conjugated polymer chains. *Sci Adv*. 2018;4:eaa05786.
- Ou H, Chen X, Lin L, Fang Y, Wang X. Biomimetic donor-acceptor motifs in conjugated polymers for promoting Exciton splitting and charge separation. *Angew Chemie Int Ed*. 2018;57:8729-8733.
- Dang D, Yu D, Wang E. Conjugated donor-acceptor Terpolymers toward high-efficiency polymer solar cells. *Adv Mater*. 2019;31:1-33.
- Jo JW, Bae S, Liu F, Russell TP, Jo WH. Comparison of two D-A type polymers with each being fluorinated on D and a unit for high performance solar cells. *Adv Funct Mater*. 2015;25:120-125.
- Kim Y, Jung EH, Kim G, Kim D, Kim BJ, Seo J. Sequentially fluorinated PTAA polymers for enhancing VOC of high-performance perovskite solar cells. *Adv Energy Mater*. 2018;8:1-9.
- Nketia-Yawson B, Lee HS, Seo D, et al. A highly planar fluorinated benzothiadiazole-based conjugated polymer for high-performance organic thin-film transistors. *Adv Mater*. 2015;27:3045-3052.
- Kim M, Ryu SU, Park SA, et al. Donor-acceptor-conjugated polymer for high-performance organic field-effect transistors: a Progress report. *Adv Funct Mater*. 2020;30:1-25.
- Jo JW, Jung JW, Jung EH, Ahn H, Shin TJ, Jo WH. Fluorination on both D and a units in D-A type conjugated copolymers based on difluorobithiophene and benzothiadiazole for highly efficient polymer solar cells. *Energ Environ Sci*. 2015;8:2427-2434.
- Cui C, He Z, Wu Y, et al. High-performance polymer solar cells based on a 2D-conjugated polymer with an alkylthio side-chain. *Energ Environ Sci*. 2016;9:885-891.
- Tsai CH, Li N, Lee CC, et al. Efficient and UV-stable perovskite solar cells enabled by side chain-engineered polymeric hole-transporting layers. *J Mater Chem A*. 2018;6:12999-13004.
- Huang H, Yang L, Facchetti A, Marks TJ. Organic and polymeric semiconductors enhanced by noncovalent conformational locks. *Chem Rev*. 2017;117:10291-10318.
- Zhao FW, Dai SX, Wu YQ, et al. Single-junction binary-blend nonfullerene polymer solar cells with 12.1% efficiency. *Adv Mater*. 2017;29:1-7.

20. Dong T, Lv L, Feng L, et al. Noncovalent se...O conformational locks for constructing high-performing optoelectronic conjugated polymers. *Adv Mater.* 2017;29:1-8.
21. Cui Y, Yao HF, Zhang JQ, et al. Over 16% efficiency organic photovoltaic cells enabled by a chlorinated acceptor with increased open-circuit voltages. *Nat Commun.* 2019;10:1-8.
22. Du Y, Yao H, Galuska L, et al. Side-chain engineering to optimize the charge transport properties of isoindigo-based random terpolymers for high-performance organic field-effect transistors. *Macromolecules.* 2019;52:4765-4775.
23. Deng P, Wu B, Lei Y, Cao H, Ong BS. Regioregular and random difluorobenzothiadiazole electron donor-acceptor polymer semiconductors for thin-film transistors and polymer solar cells. *Macromolecules.* 2016;49:2541-2548.
24. Chen S, Cho HJ, Lee J, et al. Modulating the molecular packing and Nanophase blending via a random terpolymerization strategy toward 11% efficiency nonfullerene polymer solar cells. *Adv Energy Mater.* 2017;7:1-9.
25. Duan C, Gao K, Van Franeker JJ, Liu F, Wienk MM, Janssen RAJ. Toward practical useful polymers for highly efficient solar cells via a random copolymer approach. *J Am Chem Soc.* 2016;138:10782-10785.
26. Yao HT, Li YK, Hu HW, et al. A facile method to fine-tune polymer aggregation properties and blend morphology of polymer solar cells using donor polymers with randomly distributed alkyl chains. *Adv Energy Mater.* 2018;8:1701895.
27. Gnan N, Zaccarelli E. The microscopic role of deformation in the dynamics of soft colloids. *Nat Phys.* 2019;15:683-688.
28. Nketia-Yawson B, Tabi GD, Noh YY. Polymer electrolyte blend gate dielectrics for high-performance ultrathin organic transistors: toward favorable polymer blend miscibility and reliability. *ACS Appl Mater Interfaces.* 2019;11:17610-17616.
29. Yang SF, Liu ZT, Cai ZX, et al. Diketopyrrolopyrrole-based conjugated polymer entailing triethylene glycols as side chains with high thin-film charge mobility without post-treatments. *Adv Sci.* 2017;4:1700048.
30. Zhang M, Guo X, Zhang S, Hou J. Synergistic effect of fluorination on molecular energy level modulation in highly efficient photovoltaic polymers. *Adv Mater.* 2014;26:1118-1123.
31. Jeong SH, Ahn S, Lee TW. Strategies to improve electrical and electronic properties of PEDOT:PSS for organic and Perovskite optoelectronic devices. *Macromol Res.* 2019;27:2-9.
32. Lim J, Kim NY, Jang W, et al. Selective Soxhlets extraction to enhance solubility of newly-synthesized poly(indoloindole-selenophene vinylene selenophene) donor for photovoltaic applications. *Nano Converg.* 2020;7:9.
33. Das D, Gopikrishna P, Barman D, Yathirajula RB, Iyer PK. White light emitting diode based on purely organic fluorescent to modern thermally activated delayed fluorescence (TADF) and perovskite materials. *Nano Converg.* 2019;6:1-28.
34. Jo JW, Seo MS, Park M, et al. Improving performance and stability of flexible planar-Heterojunction Perovskite solar cells using polymeric hole-transport material. *Adv Funct Mater.* 2016;26:4464-4471.
35. Shao Y, Xiao Z, Bi C, Yuan Y, Huang J. Origin and elimination of photocurrent hysteresis by fullerene passivation in CH₃NH₃PbI₃ planar heterojunction solar cells. *Nat Commun.* 2014;5:1-7.
36. Gasperini A, Wang GJN, Molina-Lopez F, et al. Characterization of hydrogen bonding formation and breaking in semiconducting polymers under mechanical strain. *Macromolecules.* 2019;52:2476-2486.
37. Marcus M, Milward JD, Köhler A, Barford W. Structural information for conjugated polymers from optical modeling. *J Phys Chem A.* 2018;122:3621-3625.
38. Kim G, Kang SJ, Dutta GK, et al. A Thienoisindigo-naphthalene polymer with ultrahigh mobility of 14.4 cm²/V·s that substantially exceeds benchmark values for amorphous silicon semiconductors. *J Am Chem Soc.* 2014;136:9477-9483.
39. Rivnay J, Steyrleuthner R, Jimison LH, et al. Drastic control of texture in a high performance n-type polymeric semiconductor and implications for charge transport. *Macromolecules.* 2011;44:5246-5255.
40. Kim J y, Park S, Lee S, et al. Low-temperature Processable high-performance D-A-type random copolymers for non-fullerene polymer solar cells and application to flexible devices. *Adv Energy Mater.* 2018;8:1-11.
41. Jo JW, Jung JW, Ahn H, Ko MJ, Jen AKY, Son HJ. Effect of molecular orientation of donor polymers on charge generation and photovoltaic properties in bulk Heterojunction all-polymer solar cells. *Adv Energy Mater.* 2017;7:1601365.
42. Nketia-Yawson B, Kang SJ, Tabi GD, et al. Ultrahigh mobility in solution-processed solid-state electrolyte-gated transistors. *Adv Mater.* 2017;29:1605685.
43. Na Y, Kim FS. Nanodroplet-embedded semiconducting polymer layers for electrochemically stable and high-conductance organic electrolyte-gated transistors. *Chem Mater.* 2019;31:4759-4768.
44. Yang HM, Kwon YK, Lee SB, Kim S, Hong K, Lee KH. Physically cross-linked Homopolymer ion gels for high performance electrolyte-gated transistors. *ACS Appl Mater Interfaces.* 2017;9:8813-8818.
45. Lee KH, Kang MS, Zhang S, Gu Y, Lodge TP, Frisbie CD. "Cut and stick" rubbery ion gels as high capacitance gate dielectrics. *Adv Mater.* 2012;24:4457-4462.
46. Nketia-Yawson B, Jung AR, Nguyen HD, Lee KK, Kim B, Noh YY. Difluorobenzothiadiazole and Selenophene-based conjugated polymer demonstrating an effective hole mobility exceeding 5 cm² V⁻¹ s⁻¹ with solid-state electrolyte dielectric. *ACS Appl Mater Interfaces.* 2018;10:32492-32500.
47. Jeong I, Jo JW, Bae S, Son HJ, Ko MJ. A fluorinated polythiophene hole-transport material for efficient and stable perovskite solar cells. *Dyes Pigm.* 2019;164:1-6.
48. Yousif QA, Agbolaghi S. A comparison between functions of carbon nanotube and reduced Graphene oxide and respective ameliorated derivatives in perovskite solar cells. *Macromol Res.* 2020;28:425-432.
49. Saliba M, Matsui T, Seo JY, et al. Cesium-containing triple cation perovskite solar cells: improved stability, reproducibility and high efficiency. *Energy Environ Sci.* 2016;9:1989-1997.
50. Soldera M, Wang Q, Soldera F, Lang V, Abate A, Lasagni AF. Toward high-throughput texturing of polymer foils for enhanced light trapping in flexible Perovskite solar cells using roll-to-roll hot embossing. *Adv Eng Mater.* 2020;22:1-9.
51. Ahmed GH, El-Demellawi JK, Yin J, et al. Giant photoluminescence enhancement in CsPbCl₃ Perovskite Nanocrystals by simultaneous dual-surface passivation. *ACS Energy Lett.* 2018;3:2301-2307.
52. Yang S, Dai J, Yu Z, et al. Tailoring passivation molecular structures for extremely small open-circuit voltage

- loss in perovskite solar cells. *J Am Chem Soc.* 2019;141: 5781-5787.
53. Cho G, Park Y, Hong YK, Ha DH. Ion exchange: an advanced synthetic method for complex nanoparticles. *Nano Converg.* 2019;6:17.

SUPPORTING INFORMATION

Additional supporting information may be found online in the Supporting Information section at the end of this article.

How to cite this article: Ko SY, Nketia-Yawson B, Ahn H, Jo JW, Ko MJ. Random copolymerization of polythiophene for simultaneous enhancement of in-plane and out-of-plane charge transport for organic transistors and perovskite solar cells. *Int J Energy Res.* 2021;45: 7998–8007. <https://doi.org/10.1002/er.6293>